Numerical Simulation of Car Tire Aquaplaning

Andrey Aksenov, Alexander Dyadkin and **Aleksey Gudzovsky**[1]

Abstract. Approach to numerical simulation of water and air flow around aquaplaning car tire is described. The approach for governing equations solving is based on a finite-volume method and non-staggered Cartesian adaptive locally refined grid. A method of subgrid geometry resolution is proposed for accurate description of curvilinear complex boundaries. This method uses a presentation of boundaries as a set of plane facets and makes CFD code compatible with CAD systems. The described technology is implemented in ***FlowVision*** code. Some results of simulation of car tire aquaplaning performed by ***FlowVision*** are presented The tire lift dependence on a tread picture is calculated.

1 INTRODUCTION

Numerical simulation of water flow around rotated car tire is one of the challenging problems for computational fluid dynamics (CFD). Main difficulties of the problem are :
- the presence of three phases - liquid, gas, rigid body - in computation domain;
- the tire motion relatively the computation domain;
- complex tire shape and large ratio between scales of tire diameter (500-1000 mm) and tread channels (2-10 mm);
- variation of tread surface under loading;
- motion of free water surface with possible water wave breaking down.

The adequate numerical method allowing to overcome all these difficulties is need to solve the problem. The main question is the choice of a grid type. The commonly used grids may be classified under non-structured grids (NSG), structured curvilinear grids (SCG) and Cartesian structured locally refined grids.

Geometry of immobile tire may be specified with high accuracy by NSG and SCG techniques. But when we need to simulate flow around rotated tire we must introduce additional numerical technique for description of tire motion in computation domain (according to coordinate system moving with car). There are two commonly used ways: the first is based on grid regeneration at each time step of numerical algorithm, and the second - on the using of sliding (overlapping) grids. The first way demands a lot of processor time for grid regeneration. The difficulties of second way are associated with low accuracy of information transfer between overlapping grids.

To solve this problem we use unmoved Cartesian adaptive locally refined grid (ALRG) coupled with subgrid geometry resolution method for description of complex tire surface and tire rotation. The advantages of this approach are: an operation with arbitrary geometry configuration, a fast grid generation, economical using of computer memory, fast grid adaptation under geometry and flow singularities, compatibility with computer aided design (CAD) systems. A gradient method is used for description of water free surface. The method is based on accurate decision of water phase transport equation by scheme with small artificial diffusion.

The described technology is implemented in CFD code ***FlowVision*** [1]. In this paper we present the main features of the proposed approach and its application for solving of car tire aquaplaning. A task of water column breaking down was also solved to determine a precision of a water-air interface dynamic simulation by ***FlowVision***.

2 METHOD OF SIMULATION

The CFD code ***FlowVision*** [1] was developed as wide-application tool for study of complex gas/fluid flows by means of numerical modeling and computer graphics.

The choice of fundamental principles underlying the ***FlowVision*** code was subjected to achieve the final goal - the user must be able to research a flow in arbitrary shaped domain containing arbitrary shaped objects with arbitrary boundary conditions on its surfaces.

Solver of ***FlowVision*** code is based on finite volume method for solving the 3D Navier-Stokes equations and equations for heat and mass transfer. Turbulence is modeled by standard k-ε model. Post-processor includes different tools for graphical representation of numerical results, such as vector (velocity) field visualization by vectors in cross sections of domain; scalar (pressure, temperature, concentration, etc.) field visualization by isolines, color flood in cross sections of domain and 3D isosurfaces of any scalar variable; visualization of flow by tracers.

FlowVision has been comprehensively tested by comparison with different experimental and numerical data [1-3].

[1] Institute for Computer Aided Design of RAS, 19/18, ul. 2-ya Brestskaia, Moscow, Russia, 123056
E-mail: FlowVision@glas.apc.org

ECCOMAS 96.
Published in 1996 by John Wiley & Sons, Ltd.

2.1 Adaptive locally refined grid

For capturing of small details of geometry, high gradients of velocities, water-air interface an adaptive local refinement of initial Cartesian grid is performed. The structure of grid with local refinement is shown in Figure 1. Resulting grid is written in memory as octree.

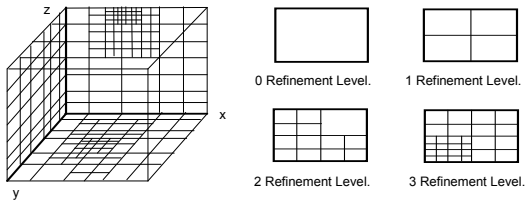

Figure 1. The structure of locally refined grid

The speed of ALRG generation is higher then ones for NSG and SCG traditionally used in CAD systems. The ALRG generation method does not produce so-called 'bad cells', because of aspect ratio of cells is constant. ALRG allows to use simply adapting technique for modelling of Navier-Stokes equations.

There are a few ways to overcome the problem of non-fittings of Cartesian ALRG to boundaries. It may be solved by first order of accuracy when object surface is formed by mesh steps. The aliasing effect takes place in this case. Higher accuracy may be achieved by local refinement of initial grid up to larger level.

But using high order techniques for boundary approximation is more accurate and demands lower expense of computer's memory and power. Such the subgrid geometry resolution method is described in the next section.

2.2 Subgrid geometry resolution method

A goal of a proposed subgrid geometry resolution method is to overcome the barrier between CAD systems and CFD code. All CAD systems can generate the description of object surface by set of plane facets. Using of this representation allows for CFD code to perceive a geometry information from CAD. Moreover in this case the CFD code becomes compatible with other CAE systems based on finite element analysis.

Let the ALGR has given in computational domain. At first stage of algorithm the facets intersecting the grid cell (Figure 2a) are being found. Then the grid cell is disjoined into a set of finite volumes bounded by facets (or facet splinters) and cell faces (or face splinters). If the cell does not intersect any facet the finite volume coincides with cell. A situation when finite volume is bounded by facet splinter only is allowable. A finite volume is indexed by i and is designated as V_i.

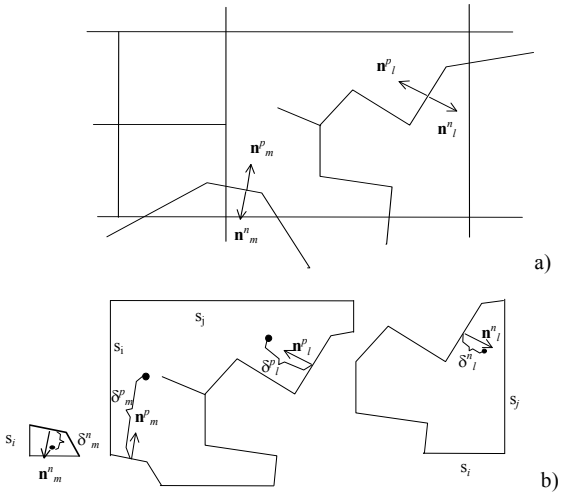

Figure 2. Subgrid geometry resolution
a) finding of facets intersected ALGR cell
b) disjoining of cell into finite volumes

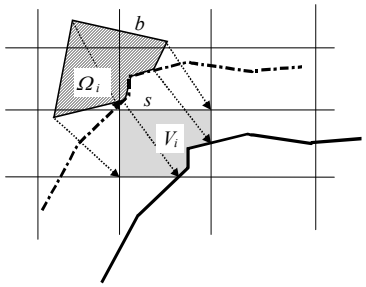

Figure 3. Displacement of i-th finite volume along backward characteristics

Introduce a volume Ω_i built on backward characteristics goes from vertexes of V_i (Figure 3). Sides of Ω_i is designated as b. Sides b of Ω_i strictly correspond to sides s of V_i.

Let write the fluid dynamics equations in Lagrange form and integrate its over moving volume which at time moment t_n coincides with Ω_i. At time $t_{n+1} = t_n + \tau$ the volume will coincide with V_i

$$f_i^{n+1} = \frac{1}{V_i}\left(\int_{\Omega_i} f^n dV + \sum_g G_g + D\right) \qquad (1)$$

where f_i^{n+1} is average of calculated variable f (component of speed, concentration, temperature and etc.) over V_i at t_{n+1}

$$f_i^n = \int_{V_i} f^{n+1} dV \qquad (2)$$

Other designations in (1) are: D - average of non-convective terms in equation (may be volumetric source, diffusion term) over the moving volume during τ, g - finite volume's side formed by the j-th facet splinter, G_g - flux of variable f through g during τ. For mixed Dirichlet-Neumann boundary conditions G_g is given by approximating expression

$$G_g = \int_{\tau}\int_{g} G_j(f)\partial s\partial t \approx \tau g(A_j + B_j(f_i^n - f_w)/\delta_g),$$

where $G_j(f)$ is a flux of f from j-th facet boundary, A_j and B_j , f_w - coefficients of a boundary condition on j-th facet, δ_g - half of characteristic distance from part of facet splinter up to other finite volume's sides in normal vector direction to a splinter (Figure 2b).

The description of the first term in right hand side of (1) which expresses a convective transfer of variable f will be done below.

2.3 One dimensional advection simulation

To build a numerical scheme for calculation of 3D convective transfer let initially consider 1D transfer of scalar f with velocity $u(x)$.

Introduce a grid with constant space step

$$x_{i+1/2}=ih, \quad i=0,1,...,N$$

where i-th finite volume are bounded by faces with coordinates $x_{i-1/2}$, $x_{i+1/2}$. Volume Ω_i corresponded to V_i is bounded by faces with coordinates $x_{i-1/2}$-$\delta_{i-1/2}$, $x_{i+1/2}$-$\delta_{i+1/2}$. Here $\delta_{i+1/2}$ is a length of a backward characteristic which goes from point $x_{i+1/2}$ at time t_{n+1} to time t_n and is determined by equation

$$\tau = \int_{x_{i+1/2}-\delta_{i+1/2}}^{x_{i+1/2}} \frac{dx}{u(x)}$$

In first approach we may consider $\delta_{i+1/2}=\tau u_{i+1/2}$.

The one dimensional advection equation written in Lagrange form is

$$f_i^{n+1} = \frac{1}{h}\int_{x_{i-1/2}-\delta_{i-1/2}}^{x_{i+1/2}-\delta_{i+1/2}} f(x,t^n)dx \qquad (3)$$

Equation (3) shows that the problem of solving of advection equation is transformed to reconstruction of function $f(x,t)$ from its averaging inside finite volumes. The monotonic reconstruction of function leads to scheme with monotonous behavior. A level of scheme artificial diffusion is determined by accuracy of $f(x)$ reconstruction.

Schemes created on the base of the Lagrange representation of advection equation (3) is stable at all time steps τ. Accuracy of time-stepping is depended on accuracy of characteristic length calculation.

Consider further different linear reconstruction inside finite volume. Various types of linear reconstruction inside finite volume are shown in Figure 4. The reconstruction I results in well known upstream scheme of the first order of approximation. The reconstruction II has an inclination $f(x)$ inside V_i calculated from central finite difference derivation. This reconstruction has the second order of approximation, but is nonmonotonous and has to result in nonmonotonous scheme.

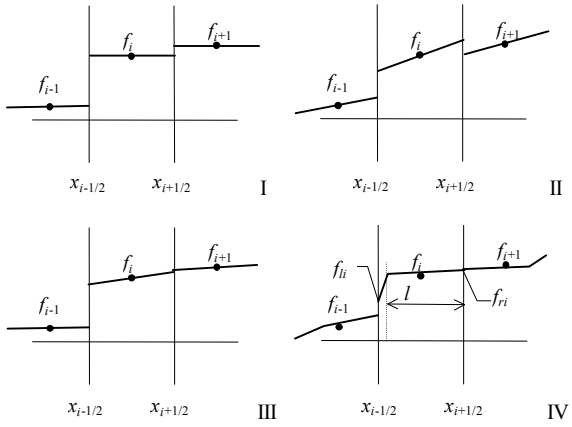

Figure 4. Types of linear reconstruction $f(x)$:
I $f(x)=f_i$;
II $f(x)=f_i+0.5(f_{i+1}-f_{i-1})(x_i-x)/h$;
III $f(x)=f_i+f_{xi}(x_i-x)/h$;
where $f_{xi} = \min(f_{i+1}-f_i, f_i-f_{i-1})$ when $f_{i+1}-f_{i-1}>0$
or $f_{xi} = \max(f_{i+1}-f_i, f_i-f_{i-1})$ when $f_{i+1}-f_{i-1}<0$;
IV linear reconstruction with additional point.

Monotonous reconstruction III is produced when inclination of $f(x)$ inside V_i is calculated from two derivations at the both sides of the finite volume.

More complex linear reconstruction with additional point (marked as IV) is used in this paper. This reconstruction is

$$f(x) = \begin{cases} f_{ri} + f_{xri}(x_{i+1/2} - x), & x \ge x_{i+1/2} - l \\ f_{li} + f_{xli}(x - x_{i-1/2}), & x \le x_{i+1/2} - l \end{cases} \qquad (4)$$

where l - is a distance from $x_{i+1/2}$ to additional point (Figure 4), f_{ri} , f_{li} - values of function reconstructed at left and right sides of finite volume

$$f_{ri} = \frac{1}{2}(f_{i+1} + f_i) - \frac{1}{6}(f_{i+1} - 2f_i + 2f_{i-1})$$
$$f_{li} = \frac{1}{2}(f_i + f_{i-1}) - \frac{1}{6}(f_{i+1} - 2f_i + 2f_{i-1})$$

Values f_{ri}, f_{li} are limited by averages in adjacent volumes:

$$\begin{cases} f_i \le f_{ri} \le f_{i+1}, & \text{when } f_{i+1} - f_i \ge 0 \\ f_i > f_{ri} > f_{i+1}, & \text{when } f_{i+1} - f_i < 0 \end{cases}$$

$$\begin{cases} f_{i-1} \le f_{li} \le f_i, & \text{when } f_i - f_{i-1} \ge 0 \\ f_{i-1} > f_{li} > f_i, & \text{when } f_i - f_{i-1} < 0 \end{cases}$$

Distance l and derivations at left and right sides of finite volume f_{xri} , f_{xli} equal to

$$l = (f_i - f_{li}) / (f_{ri} - f_{li})$$
$$f_{xri} = (f_{ri} - f_i) / l$$
$$f_{xli} = (f_i - f_{li}) / (1 - l)$$

Leonard's test problem [6] was solved to verify an accuracy of the schemes. The test consists in simulation of one dimensional motion of three test profiles (step, sine-squared and semi-ellipse) with constant velocity. Figure 5 shows the comparison of precise solution and calculated profiles by scheme produced by reconstruction I-IV after 120th time step at Courant number Cur = 0.5.

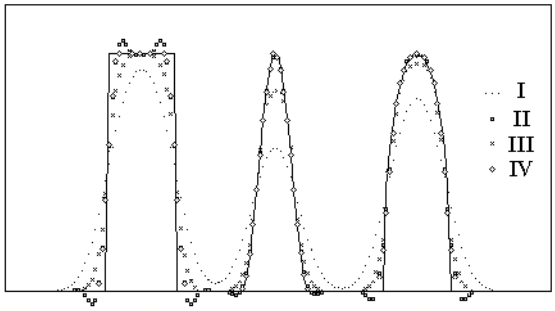

Figure 5. The simulation of motion of three test profiles by schemes I-IV (U=1, Cur=0.5, t=0.6)

One can see that the schemes I and III have inadmissible large artificial diffusion, scheme II is nonmonotonous as was predicted above. The scheme with reconstruction IV is the most accurate and has monotonous and small artificial dissipating properties.

2.4 Three dimensional transport simulation

Return to equation (1) for 3D transport. To remove a limitation on τ let disjoin the equation (1) in two equations

$$\hat{f}_i = \frac{1}{V_i} \int_{\Omega_i} f^n dV \qquad (5)$$

$$f^{n+1} = \hat{f}_i - \frac{1}{V_i}(\sum_g G_g(f^{n+1}) + D(f^{n+1})) \qquad (6)$$

The first equation (5) describes pure advection of scalar f and stable at any τ. The second equation describes diffusion process and volumetric sources (term with D), boundary effects (term with G_g). Using implicit form of (6) allows to eliminate the time step restriction for small finite volumes.

Three-dimensional function $f(\mathbf{x})$ in (5) is reconstructed from superposition of three one-dimensional reconstructions $f^{n,k}(x_k)$ along x_k axis of coordinate system

$$f^n(\mathbf{x}) = \sum_{k=1}^{3} f^{n,k}(x_k) - 2f_i^n \qquad (7)$$

Equation (6) is solved afterward finding of auxiliary scalar $\hat{f}$. This equation is written in implicit form relatively f^{n+1} and is calculated by standard methods such as successive over relaxation method.

2.5 Governing equations solving

Water and air flow around aquaplaning car tire is governed by system of equations for incompressible fluid which includes continuity and Navier-Stokes equations. To consider the algorithm of the equations solving again write ones in Lagrange integral form for volume Ω moved with fluid during τ

$$\int_{V_i} \rho dV = \int_{\Omega_i} \rho dV$$
$$\int_{V_i} \rho \mathbf{V} dV - \int_{\Omega_i} \rho \mathbf{V} dV = -\iint_{\tau, S} P d\mathbf{S} dt + \mathbf{D}$$

Here S is a surface of the volume Ω, $\mathbf{V}$ is a fluid velocity field, P - pressure, ρ - fluid density, $\mathbf{D}$ is the collection of terms in Navier-Stokes equations with viscosity stress, gravity force, and the like.

Density ρ is calculated from continuity equation using scheme (5-7)

$$\rho^{n+1} = \frac{1}{V_i} \int_{\Omega_i} \rho^n(\mathbf{x}) dV \qquad (8)$$

The algorithm of the method for solving of this equations is follows

$$\hat{\mathbf{V}}_i = \frac{1}{V_i \rho^{n+1}} \left(\int_{\Omega_i} \mathbf{V}^n dV - \tau \sum_b P_b^n \mathbf{b} \right) \quad (9)$$

$$\overline{\mathbf{V}}_i = \hat{\mathbf{V}}_i + \frac{1}{V_i} \mathbf{D}_i(\overline{\mathbf{V}}) \quad (10)$$

$$\mathbf{U}_s = \overline{\mathbf{V}}_s + \frac{\tau}{\rho_s^{n+1}} (\nabla P^n)\Big|_b \quad (11)$$

$$\sum_s \mathbf{U}_s \mathbf{s} = \sum_s \frac{\tau}{\rho_s^{n+1}} (\nabla P^n)\Big|_b \mathbf{s} \quad (12)$$

$$\mathbf{V}_i^{n+1} = \overline{\mathbf{V}}_i + \frac{\tau}{\rho_i^{n+1}} \left(\sum_b P_b^n \mathbf{b} - \sum_s P_s^{n+1} \mathbf{s} \right) \quad (13)$$

$$\mathbf{V}_s^{n+1} = \mathbf{U}_s - \frac{\tau}{\rho_s^{n+1}} (\nabla P^{n+1})\Big|_s \quad (14)$$

At first stage (9-10) finite volume's averages of intermediate velocity field $\overline{\mathbf{V}}$ are being found. Then auxiliary averages over face splinters over finite volume are calculated. The pressure field at n+1-th time step is calculated at next stage (12). This equation follows from (14) and the fact that for incompressible fluid an integral of velocity over closed surface equals to zero. At final stage (13) and (14) velocity averages over finite volume $\mathbf{V}_i^{n+1}$ and over its face's splinters $\mathbf{V}_s^{n+1}$ are calculated.

Because of a non-staggered grid is used for calculations, well known pressure field oscillations exists [4]. This difficulties is overcomed by using of Armfield's idea [5] that consist in introduction a difference between 2nd and 4th order approximations of term in (12) with pressure.

3 RESULTS

3.1 Collapse of water column

To evaluate an accuracy of the method the collapse of a water column was numerically simulated. In order to compare our solution with experimental data obtained by Martin and Moyce [7], the water column is chosen to be H×H square column (H=5.715 cm=2.5 in). The width of a channel equals to 3H. A grid 10x30 without adapting has been used for collapse simulation.

At time t=0 water column starts to collapse owing to gravity g=9.8 m/s^2. For convenience, the dimensionless time and length are defined as T=tv(g/H) and x/H, respectively. The length x is measured from left side of water column in Figure 6.

The profile of water surface at different time moments with step ΔT=0.3 is shown in Figure 6. After impacting with right side of the channel the water wave moves in opposite direction and some time later is break down.

A comparison of calculated and measured in [7] water front positions in relation to time is presented in Figure 7.

A good agreement between simulation and experiment is proved a capacity of the method to calculate free-surface problems.

3.1 Simulation of car tire aquaplaning

Numerical simulation of water flows around tire model shown in Figure 4 was performed. All calculations was made for tire with radius equals to 33 cm (13 in). The tread of 20 cm wide was specified by channels inclined to tire axis. The inclination angle ϕ was equal to 0^0, 12.5^0, 25^0. Channels depth and the water layer on road were equal to 2 cm. All calculation was made for car speed 20 m/s (76 km/h).

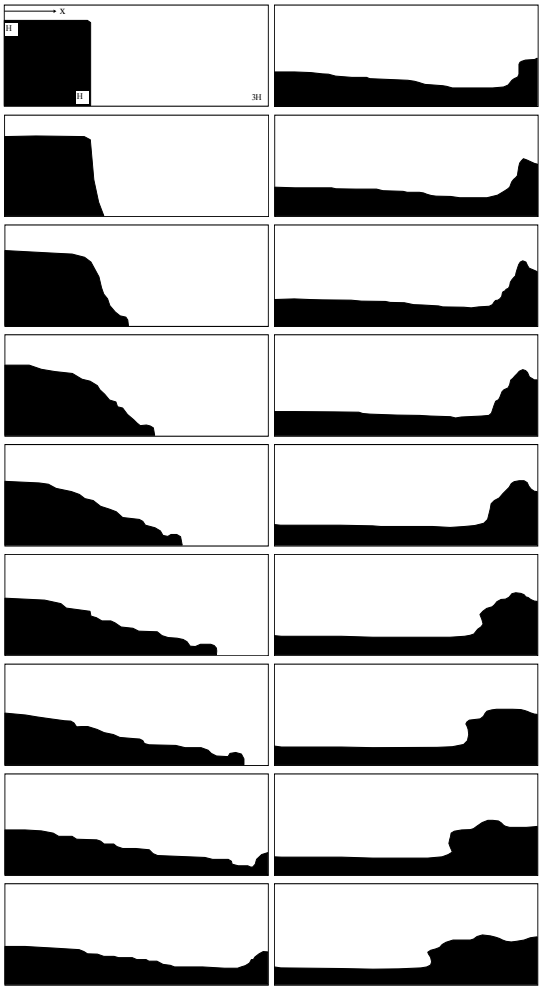

Figure 6. Predicted water surface during column collapse

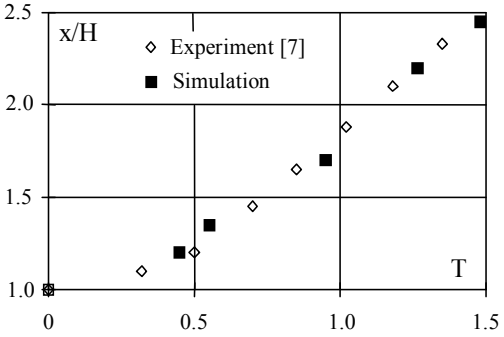

Figure 7. Front position x/H versus time T=tv(g/H) during collapse of water column

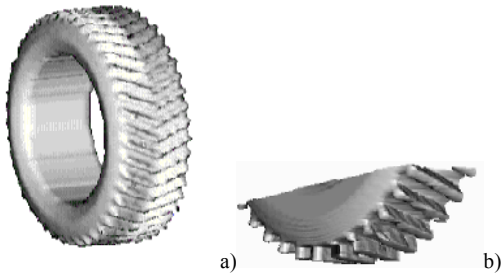

Figure 8. Tire model with inclined channels of treads. a) full view, b) calculated part

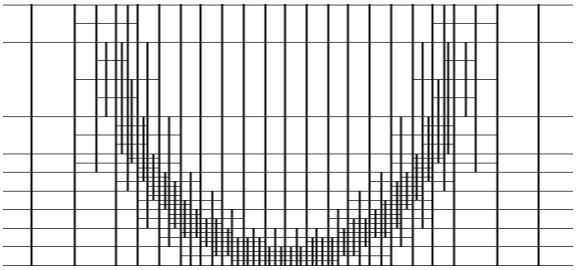

Figure 9. Locally refined grid near tread

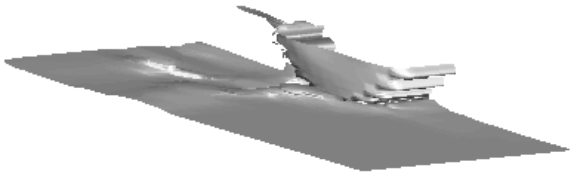

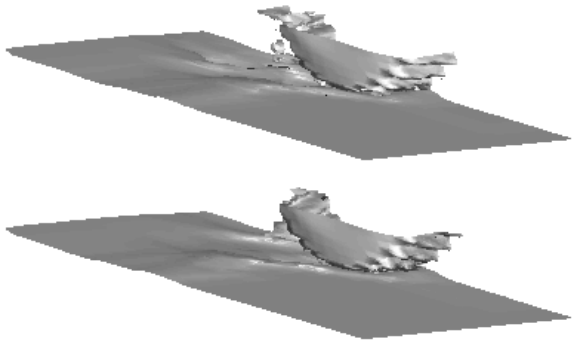

Figure 10. Water surface around the tires for $\phi = 0^0$ (a), 12.5^0 (b), 25^0 (c)

ALRG was adapted to the tread geometry. The resulting locally refined grid near tread with three refinement levels is shown in Figure 5.

The water surface disturbed by car tire is shown in Figure 6. Water surface was reconstructed from density field as shape of constant level density equals 700 kg/m^3. One can see the two waves on the water surface - bow and stern waves. There are the water jet (spray) uploaded directly behind the tire and the collapse of the water layer behind the jet.

The lift as a function of ϕ is shown in Figure 11. The increase of ϕ up to 25^o reduces the lift by 36%. As shown in Figure 11 the breaking of the tire follows to increase of the lift up to 30% for tread $\phi = 0^0$.

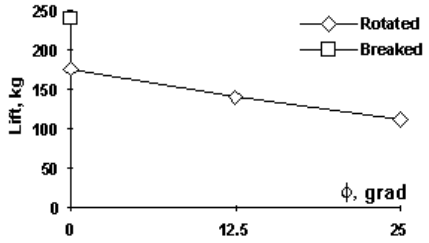

Figure 11. The tire lift against tread channels inclinations

ACKNOWLEDGEMENTS

The authors are grateful to T.Lunievski and S.Kursakov (Tesis BVBA) for support and much attention to this work. This research work has been supported in part by Russian Foundation for Fundamental Research under Grant No. 95-01-00815.

REFERENCES

[1] Aksenov, A.A., Gudzovsky, A.V., *The software **FlowVision** for study of air flows, heat and mass transfer by numerical modelling methods*, 31-35, in Proc. of the Third Forum of

Association of Engineers for Heating, Ventilation, Air-Conditioning, Heat Supply and Building Thermal Physics, 22-25 Aug. 1993, Moscow (in Russian).

[2] Aksenov A.A., Gudzovsky A.V., Serebrov A.A., *Electrohydrodynamic Instability of Fluid Jet in Microgravity*, 19-24, in Proc. of 5th Int. Symposium on Computational Fluid Dynamics (ISCFD), Aug. 31 - Sept. 3, 1993, Sendai, Japan, Japan Society of Computational Fluid Dynamics, Vol.1, 1993.

[3] Aksenov A.A., Gudzovsky A.V., Dyadkin A.A., Tishin A.P. *Gaz mixing of Low Head Jet in Crossflow*, 67-74, Izvestia of Russian Academy of Sciences, Mechanics of Fluids and Gas, 3, 1996 (in Russian).

[4] Patankar S., *Numerical heat transfer and fluid flow*, Himisphere Publishing Corporation, New York, 1980.

[5] Armfield S.W., *Finite Difference Solutions of the Navier-Stokes Equations on Staggered and Non-Staggered Grids*, 1-17, Computers Fluids, 20, N 1, 1991.

[6] Leonard B.P., *The ULTIMATE Conservative Difference Scheme Applied to Unsteady One-Dimensional Advection*, 17-74, Computer Methods in Applied Mechanics and Engineering, 88, 1991.

[7] Martin J.C., Moyce W.J., *An experimental study of the collapse of liquid columns on a rigod horizontal plane*, 312-324, Philos. Trans. Ser. A, Math. Phis. Sci., 244, 1952.